Acta Crystallographica Section A
Foundations of Crystallography
ISSN 0108-7673

Received 11 March 2009
Accepted 30 April 2009

MAD techniques applied to powder data: finding the structure given the substructure

Angela Altomare,[a] Maria Cristina Burla,[d] Corrado Cuocci,[a] Carmelo Giacovazzo,[a,b]* Fabia Gozzo,[c] Anna Moliterni,[a] Giampiero Polidori[d] and Rosanna Rizzi[a]

[a]Istituto di Cristallografia, Sede di Bari, Via G. Amendola 122/o, 70126 Bari, Italy, [b]Dipartimento Geomineralogico, Università di Bari, Campus Universitario, Via Orabona 4, 70125 Bari, Italy, [c]Swiss Light Source, Paul Scherrer Institute, CH-5232 Villigen PSI, Switzerland, and [d]Dipartimento di Scienze della Terra – Piazza Università, 06100 Perugia, Italy. Correspondence e-mail: carmelo.giacovazzo@ic.cnr.it

The joint probability distribution function method is applied to multiple-wavelength anomalous dispersion (MAD) powder data. The distributions are calculated by assuming prior knowledge of the scattering intensities at two wavelengths and of the anomalous-scatterer substructure. The method leads to formulas estimating the full structure phases and their reliability. The procedure has been applied to two structures, one unknown and one known; the second was used as a control for the phasing procedure. In spite of the unavoidable peak overlapping in the diffraction pattern, the formulas proved to be very effective. Combined with a new algorithm for phase extension, they enabled the solution of both crystal structures.

1. Notation

The following notation has been used in this article.
N: No. of atoms in the unit cell.
a: No. of anomalous scatterers in the unit cell.
$f_j = f_j^0 + \Delta f_j + if_j'' = f_j' + if_j''$: scattering factor of the jth atom. f' is its real part, f'' is its imaginary part. The thermal factor is included.
$F^+ = |F^+| \exp(i\phi^+) = F_{\mathbf{h}} = \sum_{j=1}^{N} f_j \exp(2\pi i \mathbf{hr}_j)$: structure factor of the reflection $\mathbf{h}$.
$E^+ = F^+/(\varepsilon \sum_N)^{1/2} = R \exp(i\phi^+) = A^+ + iB^+$: normalized structure factor of the reflection $\mathbf{h}$.
$F^- = |F^-| \exp(i\phi^-) = F_{-\mathbf{h}} = \sum_{j=1}^{N} f_j \exp(-2\pi i \mathbf{hr}_j)$: structure factor of the reflection $-\mathbf{h}$.
$E^- = F^-/(\varepsilon \sum_N)^{1/2} = G \exp(i\phi^-) = A^- + iB^-$: normalized structure factor of the reflection $-\mathbf{h}$.
$F_p^+, F_p^-, E_p^+ = A_p^+ + iB_p^+, E_p^- = A_p^- + iB_p^-$ denote the values for the pth wavelength.
$F_{oa} = |F_{oa}| \exp(i\phi_{oa}) = \sum_{j=1}^{a} f_j^0 \exp(2\pi i \mathbf{hr}_j)$: structure factor of the anomalous scatterers (anomalous-scattering contribution excluded).
$E_{oa} = F_{oa}/(\varepsilon \sum_{oa})^{1/2} = R_{oa} \exp(i\phi_{oa}) = A_{oa} + iB_{oa}$: normalized structure factor of the anomalous scatterers (anomalous-scattering contribution excluded).
E_p^{-*}: complex conjugate of E_p^-.
I_n: modified Bessel function of order n.
$D_1(X) = I_1(X)/I_0(X)$.

2. Introduction

While MAD (multiple-wavelength anomalous dispersion) techniques are very popular for protein crystallography, so far they have not been very useful for powder crystallography. This is mainly due to the unavoidable peak overlapping in powder patterns. Indeed:

(*a*) The reflections F^+ and F^- systematically overlap: consequently, anomalous differences $|F^+|^2 - |F^-|^2$ cannot be measured and only the intensities $I_{\mathbf{h}} = |F^+|^2 + |F^-|^2$ are experimentally available.

(*b*) Dispersive differences between $(|F_2^+|^2 + |F_2^-|^2)$ and $(|F_1^+|^2 + |F_1^-|^2)$ may be estimated from the experiment. However, the estimates may be heavily affected by the casual and/or by the systematic overlapping present in the two diffraction patterns.

The apparently minor experimental information provided by a powder diffraction experiment has discouraged the use of MAD and its applications. So far we can only quote the pioneering contributions by Prandl (1990, 1994), Gu *et al.* (2000) and Helliwell *et al.* (2005). In a more recent paper (Altomare *et al.*, 2009; from now on denoted as paper I) the probabilistic bases of the method were established. In particular it was shown that when a single species of anomalous scatterer is present:

(*a*) the distribution $P(E_{oa}, E_1^+, E_2^+, E_1^-, E_2^-)$, which is fundamental to the application to single-crystal data (Burla *et*

al., 2002, 2003), cannot be useful for powder data, owing to the fact that Bijvoet pairs cannot be separately estimated;

(*b*) $\overline{E}_p = (1/2)(E_p^+ + E_p^{-*})$ is a more suitable random variable, particularly when $|E''|^+$ (the anomalous component of $|E^+|$ using f'' as scattering factor) is negligible with respect to $|E^+|$ and $|E^{-*}|$. This occurs when f'' is sufficiently small and/or when $|E_p^+|$ and $|E_p^{-*}|$ are sufficiently large. In this case, the phase values φ_p^+ and φ_p^{-*} differ by few degrees, and the following approximation holds:

$$|\overline{E}_p| \simeq (1/2)(|E_p^+| + |E_p^{-*}|).$$

Accordingly, in paper I the joint probability distribution function $P(E_{oa}, \overline{E}_1, \overline{E}_2)$ was derived, from which the conditional distribution $P(R_{oa}|\overline{R}_1, \overline{R}_2)$ and therefore the value of $\langle R_{oa}|\overline{R}_1, \overline{R}_2\rangle$ was obtained. This value may be used as input for Patterson and direct methods to find the anomalous-scatterer substructure.

The method was successfully applied to two sets of powder diffraction data, the first originally solved by Janczak & Kubiak (2002) *via* a single-crystal experiment [iron(II) phthalocyanine bis(pyridine), $C_{32}H_{16}N_8Fe(C_5H_5N)_2$, a = 9.576, b = 19.929, c = 9.179 Å, β = 111.7°, space group $P2_1/c$, Z = 2; from now on indicated as IRON2], the second originally solved by the method described here [*trans*-dichloride-diacetateammine(1-adamantylamine)platinum(IV), $C_{14}H_{26}N_2O_4Cl_2Pt$; a = 11.100, b = 13.981, c = 6.352 Å, α = 102.3, β = 104.0, γ = 77.5°, space group $P\overline{1}$; from now on indicated as PLAT4].

In this paper we describe a probabilistic method for finding the full structure given the anomalous substructure. The method is derived for the acentric case: the final formulas may be also extended to the centric case, as shown by our applications to IRON2 and PLAT4. To simplify the calculations we neglect the effects of f'' on $\overline{E}_p$.

3. The joint probability distribution $P(R_1, R_2, R_3, \varphi_1, \varphi_2, \varphi_3)$

In the following, for simplicity, the variable $\overline{E}_p = (1/2)(E_p^+ + E_p^{-*}) = \overline{A}_p + i\overline{B}_p = \overline{R}_p \exp(i\varphi_p)$, $p = 1, 2$, will be denoted by the simpler symbol $E_p = A_p + iB_p = R_p \exp(i\varphi_p)$, $p = 1, 2$. Neglecting the effects of f'' on E_p, $p = 1, 2$, allows us to use the following simplified mathematical model:

$$A_1 = \left[\sum_{j=1}^{N} f_j^0 \cos(2\pi \mathbf{hr}_j) + |\mu_1| \cos\theta_1\right] \Big/ \left(\sum\nolimits_1\right)^{1/2}$$

$$B_1 = \left[\sum_{j=1}^{N} f_j^0 \sin(2\pi \mathbf{hr}_j) + |\mu_1| \sin\theta_1\right] \Big/ \left(\sum\nolimits_1\right)^{1/2}$$

$$A_2 = \left[\sum_{j=1}^{N} g_j \cos(2\pi \mathbf{hr}_j) + |\mu_2| \cos\theta_2\right] \Big/ \left(\sum\nolimits_2\right)^{1/2}$$

$$B_2 = \left[\sum_{j=1}^{N} g_j \sin(2\pi \mathbf{hr}_j) + |\mu_2| \sin\theta_2\right] \Big/ \left(\sum\nolimits_2\right)^{1/2}$$

$$A_3 = \left[\sum_{j=1}^{a} \Delta f_j \cos(2\pi \mathbf{hr}_j) + |\mu_3| \cos\theta_3\right] \Big/ \left(\sum\nolimits_3\right)^{1/2}$$

$$B_3 = \left[\sum_{j=1}^{a} \Delta f_j \sin(2\pi \mathbf{hr}_j) + |\mu_3| \sin\theta_3\right] \Big/ \left(\sum\nolimits_3\right)^{1/2}$$

where

$$g_j = f_j^0 + \Delta f_j \text{ for } j = 1, \ldots a, \quad g_j = f_j^0 \text{ for } j = a+1, \ldots, N,$$

$$\sum\nolimits_1 = \sum_{j=1}^{N} f_j^{0^2}, \quad \sum\nolimits_2 = \sum_{j=1}^{N} g_j^2 = \sum\nolimits_1 + \sum\nolimits_3 + 2\sum\nolimits_{13},$$

$$\sum\nolimits_3 = \sum_{j=1}^{a} \Delta f_j^2, \quad \sum\nolimits_{13} = \sum_{j=1}^{a} f_j^0 \Delta f_j.$$

$E_3 = A_3 + iB_3$ represents the normalized structure factor of the model substructure. μ_p, $p = 1, 2$, is the cumulative complex error arising from measurements and from the full pattern decomposition procedure; μ_3 represents the error on the anomalous substructure model. The role of the errors is essential for the usefulness of the mathematical approach. Indeed, if $\mu_p, p = 1, \ldots, 3$, are assumed to be zeros, the joint probability $P(R_1, R_2, R_3, \varphi_1, \varphi_2, \varphi_3)$ reduces to a Dirac delta function, owing to the fact that E_3 exactly equals $E_2 - E_1$.

In accordance with the above definitions, Δf may be assumed to be positive or negative: for example, if the first wavelength is chosen far enough from the absorption edge (to make the anomalous corrections to the structure factor negligible) and the second is chosen at the dip for f', then Δf is assumed to be negative; *vice versa* if the first wavelength is at the dip for f' and the second far away from the absorption edge then Δf is assumed to be positive.

In polar variables, the joint probability distribution $P(R_1, R_2, R_3, \varphi_1, \varphi_2, \varphi_3)$ is given by

$$P(R_1, R_2, R_3, \varphi_1, \varphi_2, \varphi_3) = (\det \mathbf{K})^{-1/2} \prod_{j=1}^{3} (\pi^{-1} R_j / e_j) \times \exp\left[-\sum_{i=1}^{3} \Lambda_{ii} R_i^2 - 2\sum_{i,j=1}^{3} \Lambda_{ij} R_i R_j \cos(\varphi_i - \varphi_j)\right], \quad (1)$$

where

$$e_j = (1 + \sigma_j^2), \ j = 1, \ldots, 3, \quad \sigma_j^2 = \langle|\mu_j|^2\rangle / \sum\nolimits_j, \ j = 1, \ldots, 3,$$

$$\sum\nolimits_{12} = \sum\nolimits_1 + \sum\nolimits_{13}, \quad \sigma_{12} = \sum\nolimits_{12} / \left(\sum\nolimits_1 \sum\nolimits_2\right)^{1/2},$$
$$\sigma_{13} = \sum\nolimits_{13} / \left(\sum\nolimits_1 \sum\nolimits_3\right)^{1/2},$$

$$\sum\nolimits_{23} = \sum_{j=1}^{a} g_j \Delta f_j = \sum\nolimits_{13} + \sum\nolimits_3, \quad \sigma_{23} = \sum\nolimits_{23} / \left(\sum\nolimits_2 \sum\nolimits_3\right)^{1/2},$$

$$\mathbf{K} = \begin{vmatrix} \mathbf{L} & 0 \\ 0 & \mathbf{L} \end{vmatrix}, \quad \mathbf{K}^{-1} = \begin{vmatrix} \mathbf{L}^{-1} & 0 \\ 0 & \mathbf{L}^{-1} \end{vmatrix},$$

$$\det \mathbf{K} = (e_1 e_2 e_3 - e_1 \sigma_{23}^2 - e_2 \sigma_{13}^2 - e_3 \sigma_{12}^2 + 2\sigma_{12}\sigma_{13}\sigma_{23})^2 / (e_1 e_2 e_3)^2,$$

$$\mathbf{L} = \begin{vmatrix} 1 & \sigma_{12}/(e_1e_2)^{1/2} & \sigma_{13}/(e_1e_3)^{1/2} \\ \sigma_{12}/(e_1e_2)^{1/2} & 1 & \sigma_{23}/(e_2e_3)^{1/2} \\ \sigma_{13}/(e_1e_3)^{1/2} & \sigma_{23}/(e_2e_3)^{1/2} & 1 \end{vmatrix},$$

$$\Lambda_{11} = \frac{1}{e_1e_2e_3\det\mathbf{L}}\left(1 - \frac{\sum_{23}^2}{\sum_2\ \sum_3}\right),$$

$$\Lambda_{22} = \frac{1}{e_1e_2e_3\det\mathbf{L}}\left(1 - \frac{\sum_{13}^2}{\sum_1\ \sum_3}\right),$$

$$\Lambda_{33} = \frac{1}{e_1e_2e_3\det\mathbf{L}}\left(1 - \frac{\sum_{12}^2}{\sum_1\ \sum_2}\right),$$

$$\Lambda_{12} = \frac{1}{e_1e_2e_3\det\mathbf{L}}\left[\frac{\sum_{13}^2 + \sum_3\ \sum_{13}(1-e_3) - \sum_1\ \sum_3 e_3}{(\sum_1\ \sum_2)^{1/2}\sum_3}\right],$$

$$\begin{aligned}\Lambda_{13} &= \big[1/(e_1e_2e_3\det\mathbf{L})\big]\big[\sum_{13}^2(1-2e_2) + \sum_3\ \sum_{13}(1-e_2) \\ &\quad + \sum_1\ \sum_{13}(1-e_2) + \sum_1\ \sum_3\big]/\big[(\sum_1\ \sum_3)^{1/2}\sum_2\big] \\ &= \big[1/(e_1e_2e_3\det\mathbf{L})\big]\big[\sum_1\ \sum_3 - e_2\sum_{13}^2 + \sum_{13}(1-e_2) \\ &\quad \times\big(\sum_{13} + \sum_1 + \sum_3\big)\big]/\big[(\sum_1\ \sum_3)^{1/2}\sum_2\big] \\ &= \big[1/(e_1e_2e_3\det\mathbf{L})\big]\big[(\sum_1\ \sum_3 - \sum_{13}^2) \\ &\quad + (1-e_2)\sum_2\ \sum_{13}\big]/\big[(\sum_1\ \sum_3)^{1/2}\sum_2\big],\end{aligned}$$

$$\Lambda_{23} = \frac{1}{e_1e_2e_3\det\mathbf{L}}\left[\frac{\sum_{13}^2 - \sum_1\ \sum_3 e_1 + \sum_1\ \sum_{13}(1-e_1)}{(\sum_2\ \sum_3)^{1/2}\sum_1}\right].$$

4. Phasing the crystal-structure reflections

In order to associate phase values to the full structure reflections we need to derive the conditional distributions $P(\varphi_1|R_1, R_2, R_3, \varphi_3)$ or $P(\varphi_2|R_1, R_2, R_3, \varphi_3)$. Such distributions cannot be obtained from equation (1) without some approximations. In accordance with Giacovazzo & Siliqi (2001) the approximation $\varphi_1 \simeq \varphi_2$ may be introduced, which is fully justified if R_1 and R_2 are sufficiently large. Then equation (1) becomes

$$P(R_1, R_2, R_3, \varphi_1, \varphi_3) \simeq 2\pi\prod_{j=1}^{3}(\pi^{-1}R_j/e_j)(\det\mathbf{K})^{-1/2} \times \exp\left[-\sum_{i=1}^{3}\Lambda_{ii}R_i^2 + G\cos(\varphi_1 - \varphi_3)\right],$$

where

$$G = -2(\Lambda_{13}R_1 + \Lambda_{23}R_2)R_3, \qquad (2)$$

and the following von Mizes conditional distribution arises:

$$P(\varphi_1|R_1, R_2, R_3, \varphi_3) \simeq [2\pi I_0(G)]^{-1}\exp[G\cos(\varphi_1 - \varphi_3)]. \quad (3)$$

From equation (2) the following rule may be deduced: if $\Lambda_{13}R_1 + \Lambda_{23}R_2$ is negative the probabilistic relation $\varphi_1 \simeq \varphi_3$ is supported. If $\Lambda_{13}R_1 + \Lambda_{23}R_2$ is positive the relation $\varphi_1 \simeq \varphi_3 + \pi$ is more probable. The probabilities are sharper when R_3 is large.

To provide a simple qualitative insight into the signs and the moduli of the Λ_{ij} we simplify their numerators by assuming that e_j for $j = 1, 2, 3$ are sufficiently close to unity: we find

$$\Lambda_{12} = -\frac{1}{e_1e_2e_3\det\mathbf{L}}\frac{Z_c}{(\sum_1\ \sum_2)^{1/2}\sum_3},$$
$$\Lambda_{13} = \frac{1}{e_1e_2e_3\det\mathbf{L}}\frac{Z_c}{(\sum_1\ \sum_3)^{1/2}\sum_2},$$
$$\Lambda_{23} = -\frac{1}{e_1e_2e_3\det\mathbf{L}}\frac{Z_c}{(\sum_2\ \sum_3)^{1/2}\sum_1},$$

where

$$Z_c = \sum_1\sum_3 - \sum_{13}^2.$$

If, as frequently occurs, the scattering power of the anomalous substructure is sufficiently smaller than that of the full structure, then:

(i) $Z_c > 0$;

(ii) Λ_{13} is positive while Λ_{12} and Λ_{23} are negative;

(iii) $\Lambda_{12}/\Lambda_{13} = -(\sum_2/\sum_3)^{1/2}$, $\Lambda_{13}/\Lambda_{23} = -(\sum_1/\sum_2)^{1/2}$, $\Lambda_{12}/\Lambda_{23} = (\sum_1/\sum_3)^{1/2}$;

(iv) $\Lambda_{23} \simeq -\Lambda_{13}$ and equation (2) reduces to

$$G \simeq 2\Lambda_{13}(R_2 - R_1)R_3. \qquad (4)$$

In other words, under the above assumptions, the reliability of the phase indication $\varphi_1 \simeq \varphi_3$ depends on the modulus R_3 and on the difference $R_2 - R_1$ [see Giacovazzo & Siliqi (2001) for a related formula]: $\varphi_1 \simeq \varphi_3$ if $R_2 > R_1$, $\varphi_1 \simeq \varphi_3 + \pi$ if $R_2 < R_1$.

It is worth noting that if Δf is assumed to be negative (*i.e.*, when the second wavelength is chosen at the dip for f'), then

$$\sum_1 > \sum_2 \text{ and } |\Lambda_{12}| > |\Lambda_{13}| > |\Lambda_{23}|.$$

If Δf is assumed to be positive (*i.e.*, when the first wavelength is at the dip for f'), then

$$\sum_2 > \sum_1 \text{ and } |\Lambda_{12}| > |\Lambda_{23}| > |\Lambda_{13}|.$$

The above results are obtained by supposing $\varphi_1 \simeq \varphi_2$. This is not always true, and therefore we look for a more accurate approach. We first integrate equation (1) on φ_2: we have

$$\begin{aligned}&P(R_1, R_2, R_3, \varphi_1, \varphi_3) \\ &\quad = 2\pi\prod_{j=1}^{3}(\pi^{-1}R_j/e_j)(\det\mathbf{K})^{-1/2}R_1R_2R_3 \\ &\qquad \times\exp\left[-\sum_{i=1}^{3}\Lambda_{ii}R_i^2 - 2\Lambda_{13}R_1R_3\cos(\varphi_1 - \varphi_3)\right]I_0(G_{13}),\end{aligned}$$

where

$$G_{13} = 2R_2[\Lambda_{12}^2R_1^2 + \Lambda_{23}^2R_3^2 + 2\Lambda_{12}\Lambda_{23}R_1R_3\cos(\varphi_1 - \varphi_3)]^{1/2}.$$

We then use the following approximation (Giacovazzo, 1979):

$$\begin{aligned}&I_0[Q_1^2 + Q_2^2 + 2Q_1Q_2\cos(\phi - \vartheta)]^{1/2} \\ &\quad = [I_0(Q_1)I_0(Q_2)/I_0(Q)]\exp[Q\cos(\phi - \vartheta)],\end{aligned}$$

where

$$D_1(Q) = D_1(Q_1)D_1(Q_2).$$

Accordingly

$$P(R_1, R_2, R_3, \varphi_1, \varphi_3) = 2\pi \prod_{j=1}^{3} \left(\frac{\pi^{-1}R_j}{e_j}\right) \frac{I_0(2\Lambda_{12}R_1R_2)I_0(2\Lambda_{23}R_2R_3)}{I_0(G_{13})} \times (\det \mathbf{K})^{-1/2} \exp\left[-\sum_{i=1}^{3} \Lambda_{ii}R_i^2 + S\cos(\varphi_1 - \varphi_3)\right],$$

where

$$S = (Q - 2\Lambda_{13}R_1R_3) \tag{5}$$

and

$$D_1(Q) = D_1(2\Lambda_{12}R_1R_2)D_1(2\Lambda_{23}R_2R_3). \tag{6}$$

Since Λ_{12} and Λ_{23} have the same sign, Q is always positive. Let us now calculate

$$P(\varphi_1|R_1, R_2, R_3, \varphi_3) = [2\pi I_0(S)]^{-1} \exp[S\cos(\varphi_1 - \varphi_3)] \tag{7}$$

from which

$$\varphi_1 \simeq \varphi_3 \text{ if } S > 0, \quad \varphi_1 \simeq \varphi_3 + \pi \text{ if } S < 0. \tag{8}$$

To understand equations (5)–(8) let us suppose that $2\Lambda_{12}R_1R_2$ is very large and negative. Then, according to equation (6), $D_1(2\Lambda_{12}R_1R_2) \simeq -1$, $Q \simeq -2\Lambda_{23}R_2R_3$, and S reduces to G, as defined by equation (2). The above result makes it clear that the assumption $\varphi_1 \simeq \varphi_2$ is only justified if $2\Lambda_{12}R_1R_2$ is large enough.

If R_1 and R_3 are large while R_2 is small, then $Q < 2\Lambda_{13}R_1R_3$ and the relation $\varphi_1 \simeq \varphi_3 + \pi$ is suggested, in accordance with equation (4).

Let us now suppose that $2\Lambda_{23}R_2R_3$ is very large and negative, as occurs in the most favourable cases. Then $D_1(2\Lambda_{23}R_2R_3) \simeq -1$ and $Q \simeq -2\Lambda_{12}R_1R_2$: in this case we have

$$S = -2\Lambda_{12}R_1R_2 - 2\Lambda_{13}R_1R_3 = -2(\Lambda_{13}R_3 + \Lambda_{12}R_2)R_1.$$

The most probable phase relationship will be $\varphi_1 \simeq \varphi_3 + \pi$ or $\varphi_1 \simeq \varphi_3$ according to whether $\Lambda_{13}R_3 + \Lambda_{12}R_2 > 0$ or $\Lambda_{13}R_3 + \Lambda_{12}R_2 < 0$, respectively. As we see, in disagreement with equation (2), the choice between the two alternatives no longer depends on the difference between R_1 and R_2 (*via* the value of $\Lambda_{13}R_1 + \Lambda_{23}R_2$), but on the difference between R_2 and R_3 (*via* the value of $\Lambda_{13}R_3 + \Lambda_{12}R_2$).

Since equations (5)–(8) have general validity, it is expected that they can provide better estimates than equations (2) and (3).

5. Simplified expressions for phase estimations

The phasing formulas described in the preceding section critically depend on the errors e_1, e_2, e_3. For example, Λ_{12}, Λ_{13} and Λ_{23} values vary with e_3, e_2, e_1: as a consequence G and S values, as defined by equations (2) and (5), respectively, will depend not only on R_1, R_2, R_3, but also on e_1, e_2, e_3. In particular, G and S may change their sign in specific circumstances. Such behaviour is in principle correct: however peak overlapping, possible preferred orientation and difficult background definition can make the error estimation quite a serious problem. In particular the Le Bail (Le Bail *et al.*, 1988) decomposition approach does not associate weights to decomposed intensities; the Pawley method, on the other hand, provides weights which may be used in the structure-refinement step (David, 2004). Suitable weights for least-squares refinement were also described by Altomare *et al.* (2006).

In general, full control of the errors in powder crystallography is more difficult than for single-crystal data. Accordingly, it may be useful to simplify the phase relationships derived in §4 in order to make them less critically dependent on the errors and, simultaneously, simpler and faster. In Appendix *A* we show that

$$e_1e_2e_3 \det(\mathbf{L}) \simeq e_3(e_1e_2 - 1)Z_c \textstyle\sum_2 \big/ \big(\sum_1 \sum_2 \sum_3\big).$$

Introducing the above relation in equation (2) gives

$$\begin{aligned} G &= -2(\Lambda_{13}R_1 + \Lambda_{23}R_2)R_3 \\ &= \frac{2\sum_3^{1/2}}{e_3(e_1e_2 - 1)\sum_2} \left(\sum_2^{1/2} R_2 - \sum_1^{1/2} R_1\right)R_3 \\ &= \frac{2}{e_3(e_1e_2 - 1)\sum_2} (|F_2| - |F_1|)|F_3| \\ &= \frac{2}{e_3(e_1e_2 - 1)} (R_2 - R_1')R_3', \end{aligned} \tag{9}$$

where R_2' and R_3' are structure factors pseudonormalized with respect to $\sum_2^{1/2}$. Equation (9) shows that the reliability parameter G assumes a very simple algebraic form when expressed in terms of structure factors or in terms of pseudonormalized structure factors. The expected value of φ_1 depends on the difference $(|F_2| - |F_1|)$; its reliability increases with $|F_3|$ and is modulated by the error function $[e_3(e_1e_2 - 1)\sum_2]^{-1}$. The larger e_1, e_2, e_3 are, the smaller the reliability of the phase indication is. Equation (9) also suggests that the accurate scaling of the intensities collected at the two wavelengths is a necessary condition for the success of the approach.

If we apply the same technique to simplify equations (5)–(7) we find that S is still defined by them, but now

$$2\Lambda_{12}R_1R_2 = -\frac{2}{e_3(e_1e_2 - 1)\sum_2} |F_1F_2| = -\frac{2}{e_3(e_1e_2 - 1)} R_1'R_2, \tag{10a}$$

$$2\Lambda_{13}R_1R_3 = \frac{2}{e_3(e_1e_2 - 1)\sum_2} |F_1F_3| = \frac{2}{e_3(e_1e_2 - 1)} R_1'R_3', \tag{10b}$$

$$2\Lambda_{23}R_2R_3 = -\frac{2}{e_3(e_1e_2 - 1)\sum_2} |F_2F_3| = -\frac{2}{e_3(e_1e_2 - 1)} R_2R_3'. \tag{10c}$$

6. Applications

The probabilistic formulas derived in §§4 and 5 were implemented in a modified version of *EXPO2004* (Altomare *et al.*,

2004): the procedure was applied to IRON2 and PLAT4 using as prior information the anomalous substructures obtained *via* the approach described in paper I. In particular, we used in the formulas the experimental $|F_1|$ and $|F_2|$ values obtained by the *EXPO2004* default full pattern decomposition procedure (Le Bail approach), and the $|F_3|$ values calculated from the known substructures. To be consistent, we report in Table 1 the experimental data quoted in Table 1 of paper I, along with the experimental data resolution (RES) for each wavelength.

In order to estimate the phases φ_1 we used both equations (2)–(3) and (5)–(7) derived in §4 and the corresponding simplified expressions [*via* equations (9) and (10)] obtained in §5. Since the two approaches did not show remarkable differences, for the sake of simplicity we will describe the results obtained *via* the simplified formulas.

The full phasing process will be described as steps.

(1) *Phasing via anomalous dispersive data*. In paper I the dispersive data were used to locate the anomalous scatterers: for IRON2 the Fe atom was found in the special position (0, 0, 0) and for PLAT4 Pt was located at (0.667, 0.311, 0.049).

We applied equation (9) to the 332 reflections lying in both measured powder patterns for IRON2 (*i.e.* up to 1.72 Å resolution): in the absence of a sound weighting criterion we assumed e_1, e_2, e_3 constantly equal to 1.05. 168 reflections were phased, with average phase error (with respect to the phases calculated from the refined crystal structure) $\langle|\Delta\varphi|\rangle = 25^\circ$ [it may be worth noting that the 168 phased reflections satisfy the relation $k + l = 2n$: indeed, since Fe is on an inversion centre, it does not contribute to the reflections with $k + l = 2n + 1$, no matter what wavelength is used]. The cumulative distribution *versus* G of the phase error is shown in Table 2.

The calculations made for IRON2 were repeated for PLAT4. We applied equation (9) to the 1289 reflections lying in both measured powder patterns (*i.e.* up to 1.14 Å resolution): 1228 reflections were phased with $\langle|\Delta\varphi|\rangle = 21^\circ$. In Table 3 we show the cumulative distribution *versus* G of the phase error.

Tables 2 and 3 indicate that the phase error distribution has the fortunate property that the wrong phase estimates are mostly confined to low values of G.

The supplementary calculations necessary to derive equations (5)–(7) are aimed at eliminating the assumption $\varphi_1 \simeq \varphi_2$, which was at the basis of equations (2) and (3). Equations (5)–(7) were then simplified *via* the relationships in equation (10) to take into account the uncertainty of the weighting criterion. We applied the simplified version of equations (5)–(7) to IRON2 and PLAT4. The cumulative phase error distributions *versus* S are shown in columns 6 and 7 of Table 2 and in columns 6 to 9 of Table 3: the use of the reliability parameter S provides slightly better results (*i.e.* the total number of wrong phase estimates is slightly smaller).

(2) *Phase extension*. Dispersive scattering allowed us to phase IRON2 reflections up to 1.72 Å and PLAT4 reflections up to 1.14 Å. To refine and extend phases we first applied the standard *EXPO* Fourier recycling procedure (Altomare *et al.*, 2006). For PLAT4 the phasing process was extended up to 1.02 Å and the procedure ended with $\langle|\Delta\varphi|\rangle = 22^\circ$ for 1826 reflections: the corresponding electron density showed 15 out of 23 peaks with $\langle d\rangle$ = 0.27 Å ($\langle d\rangle$ is the average distance between the experimental and the published atomic positions).

Table 1
Experimental data.

For each test structure the following information is given: selected wavelengths, literature values for Δf and f'' expected at the remote and at the dip (for f') wavelengths, the experimental 2θ ranges (RAN), the corresponding number of reflections (NREF), and the experimental data resolution (RES).

Code	λ (Å)	Δf	f''	RAN (2θ) (°)	NREF	RES (Å)
IRON2	1.07	0.0	0.0	1.0–40.9	464	1.54
IRON2	1.74	−8.0	0.6	1.0–60.9	332	1.72
PLAT4	0.95	0.0	0.0	1.0–55.9	1826	1.02
PLAT4	1.07	−16.0	4.0	1.0–55.9	1289	1.14

The application of the same techniques to IRON2 (phase extension from 1.72 to 1.54 Å) provided a mean phase error $\langle|\Delta\varphi|\rangle = 84^\circ$ for 464 reflections. No useful electron-density map was provided: in practice the standard *EXPO* Fourier recycling procedure spoils the extremely good phase estimates obtained *via* anomalous dispersive pairs. It was, however, noticed that the reflections with $k + l = 2n + 1$ (to which Fe does not contribute) were all phased with a very small reliability parameter. We then introduced the following new algorithm:

(*a*) Triplet invariants are calculated among the strongest reflections (NSTRONG = 220).

(*b*) A tangent procedure relying on the triplets in (*a*) is applied, by including into the starting set the phases of the reflections with $k + l = 2n$ and five symbols, represented by a magic integer sequence (Main, 1978). The procedure automatically selects the symbols among the subset of reflections for which $k + l = 2n + 1$. The corresponding trial phases are used for extending the phasing process: spoiling of the original phase estimates is avoided by holding fixed the 100 more reliable phases determined *via* anomalous dispersion effects.

(*c*) The phases obtained at the end of step (*b*) are merged with the estimates obtained by equations (5)–(7).

(*d*) The resolution bias correction procedure (Altomare *et al.*, 2008) is applied to the phases obtained at step (*c*). The algorithm cyclically corrects the truncation effects in any calculated electron-density map.

At the end of step (*d*) 464 phases were determined with $\langle|\Delta\varphi|\rangle = 34^\circ$. In the electron-density map 27 peaks out of 27 could be found with an average distance from the correct positions $\langle d\rangle$ = 0.31 Å. It is worth noting the important role of the resolution bias correction procedure: if step (*d*) is omitted, then 261 phases were determined with $\langle|\Delta\varphi|\rangle = 22^\circ$ and only 15 peaks in the final electron-density map are correctly positioned, with $\langle d\rangle$ = 0.34 Å.

(3) *Structure completion and refinement*. The Rietveld method (Rietveld, 1969) was used to complete and refine both test structures.

Table 2
Cumulative distributions of the phase error *versus* ARG for IRON2.

In columns 2 to 5 equations (2) and (3), simplified *via* equation (9), are applied. The columns 'Negative relationships' and 'Positive relationships' refer to reflections for which G [and therefore $\langle\cos(\varphi_1 - \varphi_3)\rangle$] is negative or positive, respectively. For each value of ARG the number of relationships with $|G| >$ ARG (No.) and the corresponding average phase error $\langle|\Delta\varphi|\rangle$ are given. In columns 6 and 7 equations (5) to (7), simplified *via* equations (10), are applied. In this case only negative (*i.e.* reflections for which S is negative) relationships are obtained. For each value of ARG the number of relationships with $|S| >$ ARG (No.) and the corresponding average phase error $\langle|\Delta\varphi|\rangle$ are given.

	Equations (2) and (3)				Equations (5) to (7)	
	Negative relationships		Positive relationships		Negative relationships	
ARG	No.	$\langle\lvert\Delta\varphi\rvert\rangle$ (°)	No.	$\langle\lvert\Delta\varphi\rvert\rangle$ (°)	No.	$\langle\lvert\Delta\varphi\rvert\rangle$ (°)
0.0	143	5	25	137	168	11
2.0	121	4	12	150	156	9
4.0	95	4	8	180	141	6
6.0	67	3	2	180	117	6
8.0	50	4			95	4
10.0	35	0			81	2
12.0	24	0			59	3
14.0	14	0			41	4

7. Postmortem analysis

It may be worth analyzing *a posteriori* the reasons conditioning the failure or the success of the method in order to derive useful suggestions for future work. We first notice that while accurate intensity measurements for single-crystal data are mandatory for the success of single-wavelength anomalous dispersion–multiple-wavelength anomalous dispersion (SAD–MAD) techniques (relative errors close to 5% may be critical), the need for such accuracy seems less severe for powder data if one takes into account the fact that the full pattern decomposition introduces large errors in the moduli estimates. Indeed the crystallographic residual between the true moduli and the moduli obtained by full pattern decomposition is usually large, depending on the structure size and complexity, the space-group symmetry, the experimental diffraction technique and the measurement angle 2θ. To clarify the question we calculate for each pair of variables (x, y) two types of residual,

$$\mathrm{RC} = \left(\sum_h ||y_h| - |x_h||\right) \Big/ \sum_h |y_h|$$

$$\text{and } \mathrm{RCS} = \left(\sum_h |y_h| - |x_h|\right) \Big/ \sum_h |y_h|.$$

The first is the classical crystallographic residual, the second takes into account the signs of the differences between x and y. In Fig. 1 we show the RC_i and RCS_i values for the pairs $(R_{i\mathrm{t}}, R_{i\mathrm{d}})$ for $i = 1, 2$, *versus* the interplanar spacing d: they are calculated for batches of 100 reflections sharing the same 2θ interval. $R_{i\mathrm{t}}$ is the normalized structure-factor modulus as calculated from the refined structure, $R_{i\mathrm{d}}$ is that obtained *via* full pattern decomposition. For both wavelengths RC_i increases with increasing (decreasing) values of 2θ (of d): at large 2θ values $\mathrm{R}_{i\mathrm{t}}$ and $R_{i\mathrm{d}}$ are weakly correlated for the two wavelengths. RCS_i lies around zero for both wavelengths, which indicates that $R_{i\mathrm{t}}$ and $R_{i\mathrm{d}}$ are on a similar scale, except for some 2θ intervals where systematic overestimation or underestimation of one of the two variables is made.

In Fig. 2 we show the residuals RC_Δ and RCS_Δ for the variables $y = (R_{2\mathrm{t}} - R'_{1\mathrm{t}})$ and $x = (R_{2\mathrm{d}} - R'_{1\mathrm{d}})$ [see equation (9)]. RC_Δ is always far from zero and increases with increasing values of 2θ. Since the estimate of φ_1 depends on the value of $(R_{2\mathrm{d}} - R'_{1\mathrm{d}})$ [*i.e.* if the sign of $(R_{2\mathrm{d}} - R'_{1\mathrm{d}})$ changes, then the φ_1 estimate changes by π], the dramatically large values of RC_Δ should not allow good phase estimates, in contrast with the success of our procedure. To explain this contradictory feature, we show in Fig. 2 the percentage (%inv) of reflections (per batch) for which the sign of $(R_{2\mathrm{d}} - R'_{1\mathrm{d}})$ is opposite to that of $(R_{2\mathrm{t}} - R'_{1\mathrm{t}})$. We see that, in spite of the large RC_Δ values, a remarkable sign inversion occurs only for two batches: those corresponding to the $d \simeq 1$ Å and $d \simeq 1.4$ Å intervals where RCS_2 is far from zero. This coincidental occurrence suggests that both the lack of experimental information at high-resolution 2θ intervals and a wrong background estimate may be responsible for the phase error.

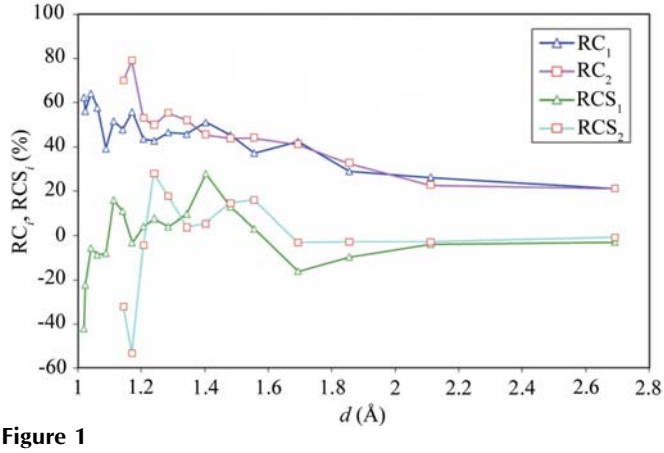

Figure 1
RC_1, RC_2, RCS_1 and RCS_2 *versus* the interplanar spacing d for PLAT4 for each batch of 100 reflections sharing the same 2θ interval.

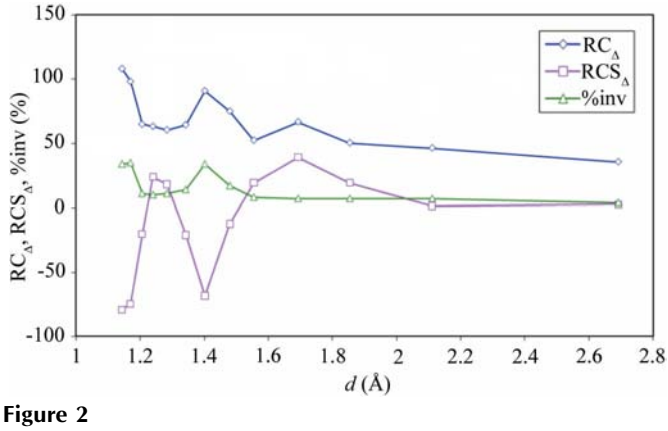

Figure 2
RC_Δ, RCS_Δ and %inv for PLAT4 for each batch of 100 reflections sharing the same 2θ interval.

Table 3
Cumulative distributions of the phase error *versus* ARG for PLAT4.

In columns 2 to 5 equations (2) and (3), simplified *via* equation (9), are applied. The columns 'Negative relationships' and 'Positive relationships' refer to reflections for which G [and therefore $\langle\cos(\varphi_1 - \varphi_3)\rangle$] is negative or positive, respectively. For each value of ARG the number of relationships with $|G| >$ ARG (No.) and the corresponding average phase error $\langle|\Delta\varphi|\rangle$ are given. In columns 6 to 9 equations (5) to (7), simplified *via* equations (10), are applied. The columns 'Negative relationships' and 'Positive relationships' refer to reflections for which S [and therefore $\langle\cos(\varphi_1 - \varphi_3)\rangle$] is negative or positive, respectively. For each value of ARG the number of relationships with $|S| >$ ARG (No.) and the corresponding average phase error $\langle|\Delta\varphi|\rangle$ are given.

	Equations (2) and (3)				Equations (5) to (7)			
	Negative relationships		Positive relationships		Negative relationships		Positive relationships	
ARG	No.	$\langle\lvert\Delta\varphi\rvert\rangle$ (°)	No.	$\langle\lvert\Delta\varphi\rvert\rangle$ (°)	No.	$\langle\lvert\Delta\varphi\rvert\rangle$ (°)	No.	$\langle\lvert\Delta\varphi\rvert\rangle$ (°)
0.0	1122	8	106	161	1185	8	43	147
2.0	815	1	44	180	938	2	8	180
4.0	592	0	24	180	785	0	3	180
6.0	397	0	18	180	627	0		
8.0	265	0	13	180	495	0		
10.0	132	0	9	180	356	0		
12.0	63	0	6	180	230	0		
14.0	34	0			143	0		
16.0	18	0			78	0		

In Fig. 3(*a*) we show, for PLAT4, the 2θ interval 37.5–39.9°, corresponding to 1.48–1.40 Å in terms of resolution, of the λ_1 PLAT4 experimental powder diffraction profile. The blue line describes the polynomial representation of the background as automatically estimated by the modified version of *EXPO2004*. The vertical blue bars in the lower part of the figure correspond to the positions of the reflections falling in that interval. It is evident that the background model is not accurate: its overestimation causes the underestimation of the reflection intensities obtained by profile decomposition, with consequent large errors in the R_{1d} estimates.

In Fig. 3(*b*) we show the 2θ interval 52.0–55.9°, corresponding to 1.22–1.44 Å resolution, of the λ_2 PLAT4 experimental powder diffraction profile. Owing to peak overlapping, uncertainty of the background and atomic scattering decay, the signal is very noisy: large errors on the R_{2t} estimates are expected, as statistically testified in Fig. 1.

From the above observations the following clues may be obtained:

(*a*) Synchrotron radiation plays a fundamental role in this technique, because it allows wavelength tuning and reduces the peak overlapping.

(*b*) The systematic overestimation or underestimation of the diffraction intensities does not necessarily lead to a sign inversion [*i.e.* when the sign of $(R_{2d} - R'_{1d})$ is opposite to that of $(R_{2t} - R'_{1t})$]. Quite frequently the full pattern decomposition mechanism overestimates or underestimates reflection intensities at both wavelengths, owing to the similarities of the two experimental diffraction profiles. As a consequence, moderately large values of RC_Δ are still compatible with good phase estimates.

(*c*) The correctness of the background modelling is much more critical for multi-wavelength than for one-wavelength powder crystallography. Indeed, in the first case the correctness of the phase assignment may depend on quite small intensity differences rather than on the full intensities.

(*d*) The signal-to-noise ratio should be carefully evaluated before deciding which experimental 2θ interval should be included in the calculations. We checked that of the 34 positive relationships with $G > 1.4$ wrongly estimated *via* equations (2) and (3), six fall in the interval shown in Fig. 3(*a*) and 27 belong to the final part of the experimental profile, shown in Fig. 3(*b*).

(*e*) Since large peak overlapping and smaller signal-to-noise ratio weaken the efficiency of the full pattern decomposition,

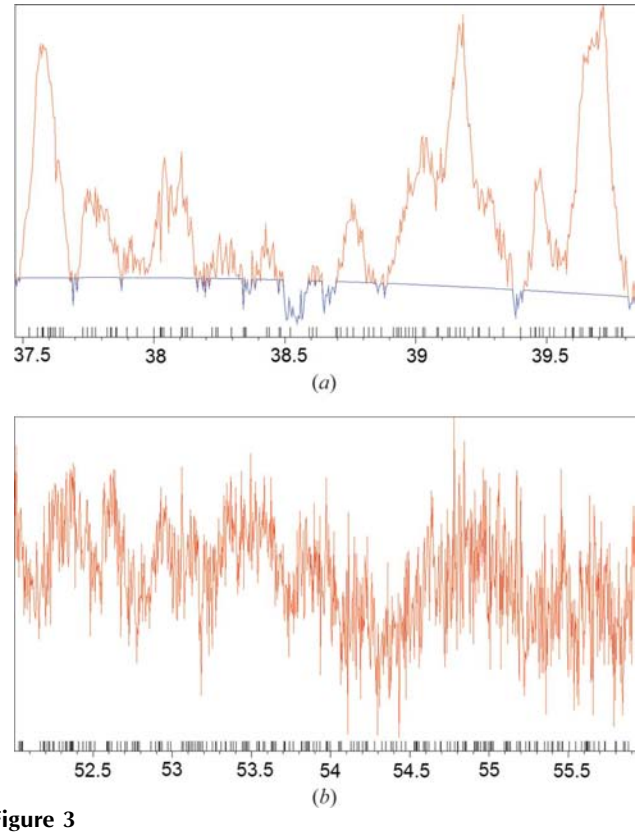

Figure 3
Experimental powder diffraction profiles for PLAT4 for: (*a*) the 2θ interval 37.5–39.9°, corresponding to 1.40–1.48 Å in terms of resolution (λ_1 wavelength); (*b*) the final 2θ interval 52.0–55.9°, corresponding to 1.22–1.44 Å resolution (λ_2 wavelength). The blue line shows the polynomial representation of the background.

Table 4
Cumulative distributions of the phase error *versus* ARG for PLAT4 assuming $e_i = 1.05[1 + (\sin^2\theta)/\lambda^2]$ for $i = 1, 2, 3$.

See Tables 2 and 3 for details.

	Equations (2) and (3)				Equations (5) to (7)			
	Negative relationships		Positive relationships		Negative relationships		Positive relationships	
ARG	No.	$\langle\lvert\Delta\varphi\rvert\rangle$ (°)	No.	$\langle\lvert\Delta\varphi\rvert\rangle$ (°)	No.	$\langle\lvert\Delta\varphi\rvert\rangle$ (°)	No.	$\langle\lvert\Delta\varphi\rvert\rangle$ (°)
0.0	1122	8	106	161	1194	8	34	153
1.0	613	0	18	180	791	0	1	180
2.0	297	0	8	180	468	0		
3.0	129	0			251	0		
4.0	47	0			118	0		
5.0	11	0			59	0		
6.0	3	0			24	0		

an angle-dependent weighting scheme may be useful. We modified the error parameters e_i, $i = 1, 2, 3$, assumed to be constant in the default applications described in §6, according to the weighting scheme

$$e_i = 1.05[1 + (\sin^2\theta)/\lambda^2] \text{ for } i = 1, 2, 3. \qquad (11)$$

We extended i up to 3 because the substructure model is expected to provide larger errors for high-resolution reflections. The integration of equation (11) into equation (9) leads to Table 4, where the cumulative distribution of the phase error *versus* $|G|$ is shown. Comparing it with the distribution shown in Table 3 suggests that the wrong phase estimates are now confined to smaller ARG values. For example, according to Table 3 there are 13 wrong phase estimates among the most reliable 265 phase relationships: in Table 4 there are only 8 wrong phase estimates among the most reliable 297 phase relationships.

Two other additional features condition the success of the procedure:

(i) The (resolution dependent) ratio $\sum_3 / \sum_1$, decisive for finding the substructure: it was very favourable for both our test cases, for which $|\Delta f| \geq 8$. In cases where the anomalous scatterers are not as heavy and the structure size is larger, the ratio $\sum_3 / \sum_1$ may become critical.

(ii) The ratio 'scattering power of the anomalous substructure/scattering power of the full structure': in both our test cases this ratio was particularly high, but it becomes critical when it is relatively small. Indeed, in this last case the experimental noise may overcome the signal, with a consequent increase in the percentage of sign inversions.

We leave this study to future investigations.

8. Conclusions

The method of joint probability distribution functions has been successfully applied to two-wavelength powder data affected by anomalous dispersion: assumptions were made which allow one to disregard the f''component. The mathematical approach provided two types of formulas for estimating the phases of a crystal structure when the anomalous substructure is known. The first type [equations (2) and (3)] requires an approximation that is not always guaranteed, the second [equations (5)–(7)] is expected to be valid in more general conditions. Both were simplified without loss of efficiency by introducing useful approximations in the errors. When applied to the experimental data of two crystal structures all the formulas provided useful phase estimations.

It is worth noting that since a general assumption allows one to neglect the f'' component, the final formulas derived above may be applied to isomorphous replacement.

APPENDIX *A*
Explicit expression for $e_1e_2e_3\det(\mathbf{L})$

In order to derive simpler formulas for phase estimation we calculate the explicit expression of $e_1e_2e_3\det(\mathbf{L})$. We obtain

$$\begin{aligned} &e_1e_2e_3\det(\mathbf{L}) \\ &= e_1e_2e_3\big(e_1e_2e_3\textstyle\sum_1\sum_2\sum_3 - e_1\sum_{23}^2\sum_1 - e_2\sum_{13}^2\sum_2 \\ &\quad - e_3\sum_{12}^2\sum_3 + 2\sum_{12}\sum_{13}\sum_{23}\big)\big/\big(e_1e_2e_3\textstyle\sum_1\sum_2\sum_3\big) \\ &= \{\textstyle\sum_1\sum_3\big[e_3(e_1e_2-1)\sum_1 + e_1(e_2e_3-1)\sum_3 \\ &\quad + 2(e_1e_2e_3 - e_1 - e_3 + 1)\sum_{13}\big] - \sum_{13}^2\big[(e_1+e_2-2)\sum_1 \\ &\quad + (e_2+e_3-2)\sum_3 + 2(e_2-1)\sum_{13}\big]\}\big/\big(\textstyle\sum_1\sum_2\sum_3\big). \end{aligned} \qquad (12)$$

Equation (12) clearly shows that $\det(\mathbf{L})$ vanishes when $e_i = 0$ for $i = 1, 2, 3$, as theoretically anticipated in the main text. Each of the terms in the numerator of equation (12) contains a polynomial which depends on the e_i values: each polynomial is different from the others but all are non-negative definite, and all increase when the e_i's increase. Since e_i's are supposed to be small, we may approximate all the polynomials by a unique non-negative expression, *e.g.* $e_3(e_1e_2 - 1)$. Then equation (12) may be approximated by

$$\begin{aligned} e_1e_2e_3\det(\mathbf{L}) &\simeq \big(\textstyle\sum_1\sum_3 - \sum_{13}^2\big)e_3(e_1e_2-1) \\ &\quad \times \big(\textstyle\sum_1 + \sum_3 + 2\sum_{13}\big)\big/\big(\sum_1\sum_2\sum_3\big) \\ &= \big(\textstyle\sum_1\sum_3 - \sum_{13}^2\big)e_3(e_1e_2-1) \\ &\quad \times \textstyle\sum_2\big/\big(\sum_1\sum_2\sum_3\big) \\ &= e_3(e_1e_2-1)Z_c\textstyle\sum_2\big/\big(\sum_1\sum_2\sum_3\big), \end{aligned}$$

where

$$Z_c = \big(\textstyle\sum_1\sum_3 - \sum_{13}^2\big).$$

We acknowledge the Paul Scherrer Institute for provision of the Swiss Light Source synchrotron radiation facility.

References

Altomare, A., Belviso, B. D., Burla, M. C., Campi, G., Cuocci, C., Giacovazzo, C., Gozzo, F., Moliterni, A., Polidori, G. & Rizzi, R. (2009). *J. Appl. Cryst.* **42**, 30–35.
Altomare, A., Caliandro, R., Camalli, M., Cuocci, C., Giacovazzo, C., Moliterni, A. G. G. & Rizzi, R. (2004). *J. Appl. Cryst.* **37**, 1025–1028.
Altomare, A., Cuocci, C., Giacovazzo, C., Moliterni, A. & Rizzi, R. (2008). *J. Appl. Cryst.* **41**, 592–599.
Altomare, A., Cuocci, C., Giacovazzo, C., Moliterni, A. G. G. & Rizzi, R. (2006). *J. Appl. Cryst.* **39**, 558–562.
Burla, M. C., Carrozzini, B., Cascarano, G. L., Giacovazzo, C. & Polidori, G. (2003). *Acta Cryst.* D**59**, 662–669.
Burla, M. C., Carrozzini, B., Cascarano, G. L., Giacovazzo, C., Polidori, G. & Siliqi, D. (2002). *Acta Cryst.* D**58**, 928–935.
David, W. I. F. (2004). *J. Appl. Cryst.* **37**, 621–628.
Giacovazzo, C. (1979). *Acta Cryst.* A**35**, 757–764.
Giacovazzo, C. & Siliqi, D. (2001). *Acta Cryst.* A**57**, 700–707.
Gu, Y. X., Liu, Y. D., Hao, Q. & Fan, H. F. (2000). *Acta Cryst.* A**56**, 592–595.
Helliwell, J. R., Helliwell, M. & Jones, R. H. (2005). *Acta Cryst.* A**61**, 568–574.
Janczak, J. & Kubiak, R. (2002). *Inorg. Chim. Acta*, **342**, 64–76.
Le Bail, A., Duroy, H. & Fourquet, J. L. (1988). *Mater. Res. Bull.* **23**, 447–452.
Main, P. (1978). *Acta Cryst.* A**34**, 31–38.
Prandl, W. (1990). *Acta Cryst.* A**46**, 988–992.
Prandl, W. (1994). *Acta Cryst.* A**50**, 52–55.
Rietveld, H. M. (1969). *J. Appl. Cryst.* **2**, 65–71.